Microsecond wide-field TCSPC microscopy based on an ultra-fast CMOS camera

Liisa M. Hirvonen,[a] Zdeněk Petrášek,[b] Andrew Beeby[c] and Klaus Suhling[a]

[a]Department of Physics, King's College London, Strand, London WC2R 2LS, U.K.

[b]Institut für Biotechnologie und Bioprozesstechnik, Technische Universität Graz, Petersgasse 10-12/I, 8010 Graz, Austria

[c]Department of Chemistry, University of Durham, Durham DH1 3LE, U.K.

ABSTRACT

Ultra-fast frame rate CMOS cameras, combined with a photon counting image intensifier, can be used for microsecond resolution wide-field time-correlated single photon counting (TCSPC) microscopy. A sequence of frames is recorded after an excitation pulse, and the number and location of photons in each frame is determined. This process is repeated until enough photons are recorded for a photon arrival time histogram in the pixels of the image. This approach combines low, nanowatt excitation power with single-photon detection sensitivity and arrival timing in many pixels simultaneously, short acquisition times in the order of seconds and allows lifetime mapping with a time resolution of ∼1 microsecond. Moreover, we also show that the phosphor decay can be exploited to time the photon arrival well below the exposure time of the camera. This approach yields better time resolution and larger images than direct imaging of photon events. We show that both methods are ideal for lifetime imaging of transition metal compounds in living cells within a few seconds.

Keywords: Phosphorescence lifetime imaging (PLIM), Time-correlated single photon counting (TCSPC), Fluorescence lifetime imaging (FLIM), Image intensifier, Microchannel plate (MCP), Phosphor, Phosphorescence

1. INTRODUCTION

Long-lifetime probes are useful especially in biological imaging, where time-resolved acquisition allows the discrimination between fast-lived autofluorescence of the sample and the long lifetime signal from the probe.[1] In recent years, there has been much interest in the development of transition metal probes,[2,3] whose typical lifetimes from hundreds of nanoseconds to a few microseconds allow faster data collection than conventional lanthanide probes with milliseconds lifetimes.[4,5] These probes are usually bright, chemically stable and water soluble, and absorb in the visible spectrum with large Stokes shift and tunable emission. Many phosphorescent d-block complexes are quenched by molecular oxygen, making them useful as minimally invasive optical oxygen sensors.[6–8] Phosphorescence lifetime imaging (PLIM) of transition metal complexes has also been used for the study of air-flow and pressure in aerodynamic studies, also known as luminescent barometry.[9] Additionally, the measurement of polarization-resolved microsecond lifetimes allows the determination of the rotational diffusion of large molecular weight proteins or other macromolecules,[10] and can be used for stepwise observation of cleavage or binding.[11]

Time-correlated Single Photon Counting (TCSPC) is a mature and the most reliable, sensitive and precise technique to measure photon arrival times. In fluorescence microscopy, TCSPC is often implemented in confocal or multiphoton excitation scanning fluorescence lifetime imaging (FLIM) systems. This has the advantage of optical sectioning, but for microsecond lifetimes the long pixel dwell times can make the data acquisition slow. Furthermore, some imaging modalities, such as total internal reflection (TIRF), supercritical angle fluorescence (SAF) and light-sheet microscopy, are difficult to carry out with scanning and require a position-sensitive detector. Wide-field FLIM can be realised in the time domain by taking wide-field time-gated "snapshots" of the fluorescence emission at various nanosecond delays after the excitation, or in the frequency domain using a

Further author information: Corresponding author email: klaus.suhling@kcl.ac.uk

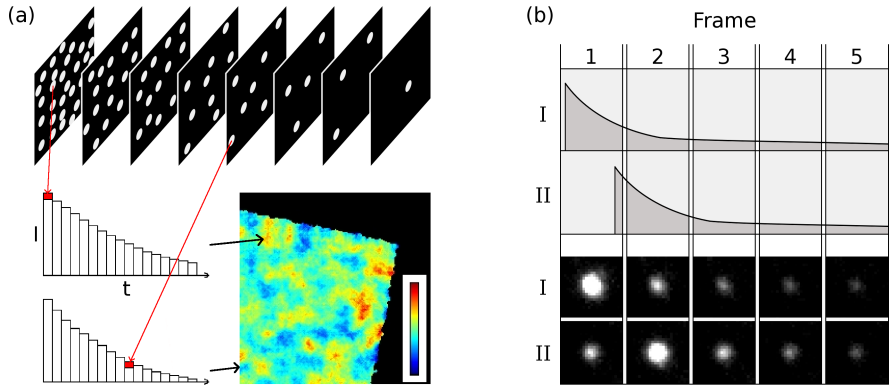

Figure 1. (a) Principle of wide-field TCSPC data acquisition to measure luminescence decays. After each excitation pulse, a sequence of frames is acquired; this process is repeated many times. The location of the photons and the arrival time (frame number) after excitation are extracted by software to build up an arrival time histogram for each pixel of the image, i.e. a 3D data cube in x, y and t. A lifetime image is built by fitting an appropriate exponential decay function to the arrival time histogram in each pixel, and encoding the lifetime in a pseudocolor scale. (b) Time resolution can be improved by using an intensifier with a phosphor that has a longer decay time which allows the photon events to be seen in many consecutive frames. The sample is excited at the beginning of each frame exposure, and the arrival time is found from the relative intensities in the first two frames where the event is detected. Photon I arrives at the beginning of frame 1 and most of the intensity from the phosphor decay is in this frame, whereas for photon II arriving at the end of the frame the second frame is brightest.

sinusoidally modulated excitation beam and detector.[12] These approaches are fast, but they usually require a signal level high enough so it is practically possible to gate or modulate it.[13]

Wide-field TCSPC can be performed with ultra-fast frame rate cameras in combination with an image intensifier operated with saturated gain.[14,15] This allows single photon events to be detected at high frame rates up to 1 MHz.[15] After each excitation pulse, a sequence of frames is acquired during the decay time, and by repeating this process many times, a histogram of the photon arrival times is built for each pixel of the sensor (Fig 1a). The temporal response of MCP-based intensifiers can be fast (<20 ps[16]) and the system has no dead-time during which photons get lost. The time resolution is limited by the frame rate of the camera – currently to ∼1 μs with commercially available cameras – but this method allows the parallel acquisition of photons in each pixel of the sensor. This time resolution is high enough to image some transition metal probes,[3,8] and can be improved by exploiting the phosphor decay of the image intensifier screen.

In an image intensifier, the incoming photon hits a photocathode and creates a photoelectron, which is then accelerated through microchannel plates (MCPs), creating an electron cloud. The electrons are converted back into photons when they hit a phosphor screen. The phosphor screen decay time depends on the type of phosphor and can range from nano- to milliseconds. Usually this afterglow is undesired,[17] but we have shown that it can be exploited to find the photon arrival time within the frame exposure time.[18,19] If the phosphor decay time is long enough for the photon events to be detected in multiple frames, the photon arrival time within the frame exposure time can be determined from the relative intensities of the photon events in subsequent frames (Fig 1b).[18] A similar approach has been used for ion velocity mapping,[20,21] a time-of-flight mass spectroscopy method to measure ion fragments.[22]

In this work, we have employed our wide-field TCSPC system to image the microsecond decay times of iridium compounds. We then show how the phosphor decay of the image intensifier can be exploited for accurate timing of photon arrival well below the camera exposure time.

2. MATERIALS AND METHODS

2.1 Data acquisition

A diagram of the experimental setup is shown in Fig 2a. A Photron Fastcam SA5 or SA1.1 CMOS camera (Photron, CA) was used for image acquisition. A pulsed 467 nm (PLP-10, Hamamatsu, Japan; 90 ps pulse

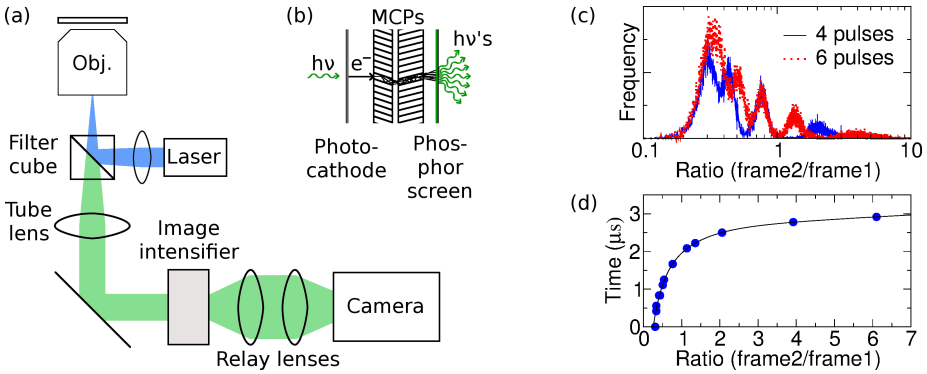

Figure 2. (a) Diagram of the experimental setup. The image intensifier was mounted to the side port of an inverted microscope, and the intensifier output screen imaged onto the camera using two relay lenses. (b) In an image intensifier an incoming photon ($h\nu$) hits the photocathode creating a photoelectron (e^-), which is multiplied while travelling through the MCP, and the resulting electron cloud is converted back to photons when it reaches the phosphor screen. (c-d) Example measurement of ratio-to-time conversion function for phosphor decay method at 300 kHz camera frame rate. By triggering the laser multiple times during the exposure, a frequency histogram of the ratio between the second and the first detection of the photon events has peaks at the laser trigger positions (c). The conversion function was obtained by plotting the peak positions against the laser trigger times, and fitting it with a 3-exponential function (d).

width) or 375 nm (DeltaDiode, Horiba, U.K.; 45 ps pulse width) diode laser was used for illuminating the sample. For direct measurement, the camera was triggered from the laser, collecting a defined number of frames after each excitation pulse. For the phosphor decay method, the laser was triggered from the camera once during each exposure with a delay. Two 40 mm diameter dual proximity-focused image intensifiers (Photek, U.K.) were used: either a 2-MCP intensifier with a P47 phosphor for direct measurements, or a 3-MCP intensifier with P20 phosphor for the phosphor decay method measurements. The intensifier, operating in photon counting mode[23,24] was mounted on the side port of an inverted microscope (Eclipse TE2000-U, Nikon, Japan). The objective was a 4× 0.13NA or 10× 0.3NA air objective (Nikon, Japan). A green (Nikon, Japan; ex:480/30nm, DM:505nm, em:515LP) or blue (Nikon, Japan; ex:350/50nm, DM:400nm, em:442LP) filter cube was used for separating the excitation and emission light. The phosphor screen of the intensifier was imaged onto the camera using two 50 mm focal length photographic lenses (F=1/1.2, Canon, Japan and F=1/1.4, Nikon, Japan).

2.2 Ratio-to-time conversion

To convert the measured intensity ratio to arrival time with the phosphor decay method, a conversion function was determined experimentally with two different methods. The camera was set to trigger the laser multiple times,[19] or once with a variable time delay,[25] during each frame exposure. A mirror was placed on the sample stage and the emission filter was removed, allowing the detection of photons from the reflected laser pulses. For each detected photon, the ratio between the second and the first detection was added into a frequency histogram. The histogram has peaks at the laser trigger positions. For multiple pulses per frame these are equally spaced in time depending on the frame rate and the number of pulses in the frame (see Fig 2c), and for one pulse/frame the peak is found at the time delay position after the exposure start time. The ratio peak positions were found by a Gaussian fit to the peak area, plotted against the trigger times, and fitted with a triple-exponential function, as shown in Fig 2d. This function is used for converting the measured photon intensity ratio to arrival time.

2.3 Data processing

For the direct measurement, the data was saved in 8-bit raw format. The frames were thresholded, and areas that had more than four adjacent pixels above the threshold were counted as photon events. The brightest pixel of this area was recorded as the photon event center pixel, and the photon arrival time (frame number) was recorded in a histogram for that pixel (see Fig 1a).

For the phosphor decay method, the frames were saved in 16-bit raw format. The frames were first thresholded, and the background was subtracted. Areas that had between eight and 300 adjacent pixels above the

threshold were counted as photon events. The brightest pixel of this area was recorded as the event centre pixel, and the total area and intensity of the event were determined. The software then checked whether an event had been detected at the same position in the previous frame. If the event was detected in at least three subsequent frames with the ratio of the third and the second detection in the expected range consistent with a decaying photon event rather than a new one, the ratio of the second and the first detection was recorded in a histogram. The ratio was then converted to time using the experimentally determined conversion function (Fig 2d).

For both methods, the resulting arrival time histograms (time decays) were fitted with TRI2 software[26,27] using a Levenberg-Marquardt fitting routine.

2.4 Sample preparation

Polystyrene beads (200 μm diameter) were swollen by suspension in dichloromethane and then soaked in dicholoromethane solutions of iridium complexes $Ir(BMes_2)_2acac$,[28] $Ir(ppy)_3$ and $Ir(fppy)_3$,[29] palladium ocatethylporphine (Pd(OEP), Sigma-Aldrich, U.K.) and 9,10-bis(phenylethynyl) anthracene (BPEA). After soaking for 30 minutes the supernatant solution was decanted and the beads washed with ethanol, which causes them to shrink and trap the dyes inside the particles. After thorough washing with ethanol the beads were air dried and placed on #1.5 coverslips for imaging. Ruthenium compound bis(2,2-bipyridine)-(5-isothiocyanatophenanthroline)ruthenium bis(hexafluorophosphate) $(Ru(bpy)_2(phen\text{-}5\text{-}isothiocyanate)(PF_6)_2$, Sigma-Aldrich, U.K.) was mixed with water and deposited on a multiwell plate with #1.5 coverslip bottom for imaging. For the cell samples, Ruthenium-tris(4,7-diphenyl-1,10-phenanthroline) dichloride $(Ru(dpp)_3Cl_2$, Sigma-Aldrich, U.K.) was mixed with 300 μl of DMEM (Sigma-Aldrich, U.K.) and added to the medium of HeLa cells grown on #1.5 coverslip glass bottom dishes (Thistle Scientific, U.K.). The cells were incubated at 37°C overnight, washed twice with OptiMEM (Sigma-Aldrich, U.K.), then imaged in OptiMEM.

3. RESULTS

3.1 Lifetime imaging of Ir compounds

Wide-field TCSPC lifetime images of the iridium beads are shown in Fig 3a. The images were acquired with a 4× objective and camera frame rate of 675,000 Hz which allows a maximum image size of 64×16 pixels. The excitation laser repetition rate was 10 kHz, with 15 frames collected after each laser pulse. The data sets consist of ∼400,000 frames with ∼37,000 photons and a total image acquisition time of less than 1 s for each sample. The histograms of individual pixel lifetimes have a Gaussian shape (Fig 3b). Monoexponential fits to the data sets with all pixels binned yield lifetimes of ∼0.9 μs, ∼1.3 μs and ∼1.3 μs for the $Ir(ppy)_3$, Ir(BMes) and $Ir(fppy)_3$ complexes, respectively (Fig 3c). The lifetime of BPEA could not be measured with this method, as the fluorescence lifetime of a few nanoseconds yields only one time data point.

Lifetime images of the same iridium beads measured with the phosphor decay TCSPC method and 10× objective are shown in Fig 3d, with histograms of pixel lifetimes in Fig 3e. The lower frame rate of 54 kHz allows a bigger image size – here 128×128 pixels were used instead of the maximum 256×256 pixels. A 5 μs delay was used for the excitation pulse. A total of 70,000 frames with an average of ∼41,000 photons were collected for each sample, with a total data acquisition time of 1.3 s/sample. Fig 3f shows the time decays for the images with all pixels binned together. The instrument response function (IRF), measured with reflection, was deconvolved from the time decays, which were then fitted with a monoexponential decay law. This yields lifetimes of ∼0.8 μs, ∼1.1 μs and ∼1.2 μs for the $Ir(ppy)_3$, Ir(BMes) and $Ir(fppy)_3$ complexes, respectively, and ∼0.3 μs for the fluorescent BPEA.

Table 1. Luminescence lifetimes of the Ir compounds infused in beads. Lifetime τ_1 was obtained from a conventional wide-field TCSPC measurement and τ_2 with wide-field TCSPC from the photon event phosphor decay.

	$Ir(ppy)_3$	Ir(BMes)	$Ir(fppy)_3$	BPEA
τ_1 (Direct measurement)	∼0.9 μs	∼1.3 μs	∼1.3 μs	-
τ_2 (Phosphor decay)	∼0.8 μs	∼1.1 μs	∼1.2 μs	∼0.3 μs

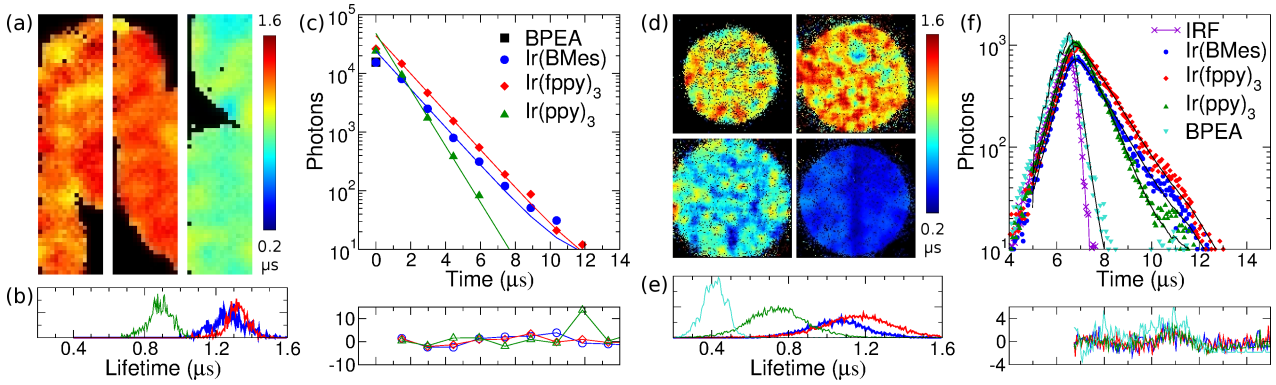

Figure 3. (a) Lifetime images of beads with $Ir(ppy)_3$, Ir(BMes) and $Ir(fppy)_3$ complexes (from left to right, respectively), imaged with direct TCSPC measurement with 675,000 Hz camera frame rate. (b) Histograms of the individual pixel lifetimes in (a). (c) Time decays of images in (a) with all pixels binned, monoexponential fits to the data and residuals. (d) Lifetime images of beads with $Ir(ppy)_3$ (top left), Ir(BMes) (top right), $Ir(fppy)_3$ (bottom left) complexes and BPEA (bottom right), imaged with phosphor decay method and 54 kHz camera frame rate. (e) Histograms of the individual pixel lifetimes in (c). (f) Time decays of images in (c) with all pixels binned (data points), monoexponential fits to the data (lines) and residuals.

3.2 Lifetime imaging of Ru compounds

The intensity and lifetime images of a Ru compound $Ru(bpy)_2(phen\text{-}5\text{-}isothiocyanate)(PF_6)_2$ in a multiwell plate, imaged with 4× objective and 375 nm laser, are shown in Fig 4a. The faster camera frame rate of 300 kHz allowed a maximum image size of 256×64 pixels. The excitation pulse delay was set to 700 ns after the frame start time. The data set consists of a total of 370,000 frames and 37,000 photons, acquired in 1.2 s. The IRF was deconvolved from the decay of all pixels binned together, which was then fitted with a monoexponential decay law (Fig 4c). This yields a lifetime of 456±4 ns, which is in reasonable agreement with a previously quoted lifetime of ∼490 ns.[30]

The lifetime of another Ru compound, $Ru(dpp)_3^{2+}$, was measured in living HeLa cells (Fig 4d-f). The compound was found to be distributed in the cytoplasm after overnight incubation. Due to the cellular autofluorescence, the decay has a fast component and was fitted with a double-exponential function (Fig 4f). The average lifetime of $Ru(dpp)_3^{2+}$ was found to be 2.95 μs, with a fast component of 0.04 μs attributable to the cellular autofluorescence. There are no systematic deviations in the residuals, indicating a good fit, and a lifetime distribution histogram has a Gaussian shape (Fig 4e, inset). The lifetime of $Ru(dpp)_3^{2+}$ is longer than in water, in agreement with previous work[15,19] and indicating partial protection from quenching by molecular oxygen. The total data acquisition time was 2.6 s, during which 140,000 frames and 134,000 photons were collected, with a mean count rate of 52,000 photons/s.

4. DISCUSSION

This work describes two methods using ultra-fast frame rate cameras in combination with a photon counting image intensifier for wide-field TCSPC lifetime imaging. Lifetimes of iridium complexes infused in polystyrene beads were measured with both methods. The results are in agreement, although the lifetimes measured with the direct method are slightly longer than the lifetimes measured with the phosphor decay method. With the direct method there are not many data points to fit, and the image size was limited to 64×16 pixels. The phosphor decay method with 54 kHz camera frame rate allows the measurement of lifetimes from a few hundred of nanoseconds to a few microseconds with maximum image size of 256×256 pixels. This frame rate was chosen for expected lifetimes around 1 μs (Ir complexes) to a few μs ($Ru(dpp)_3^{2+}$ in cells). A faster frame of 300 kHz was chosen for the measurement of $Ru(bpy)_2(phen\text{-}5\text{-}isothiocyanate)(PF_6)_2$ in water, where the expected lifetime was around 500 ns – three times faster than the maximum inverse frame rate (675 kHz) of the camera. The measurement time interval is adjustable and faster frame rates allow the measurement of shorter decays, but

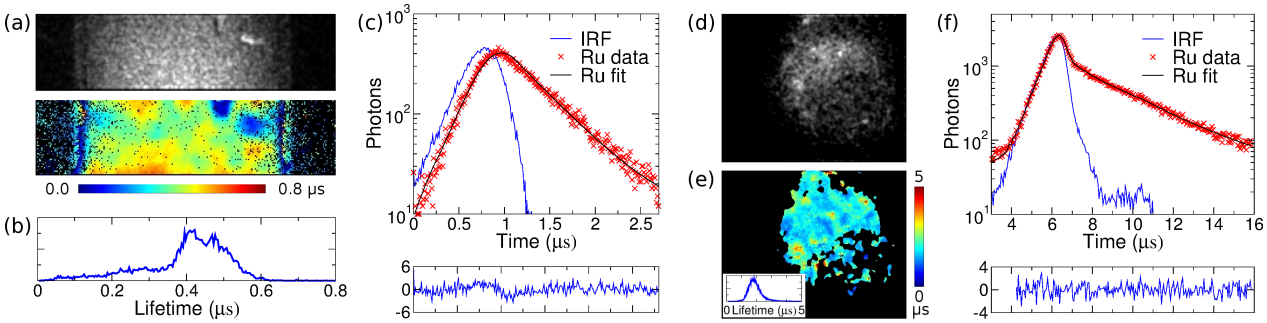

Figure 4. (a-c) Ruthenium compound $Ru(bpy)_2(phen\text{-}5\text{-}isothiocyanate)(PF_6)_2$ imaged with phosphor decay TCSPC at 300 kHz. (a) Intensity (top) and lifetime (bottom) images of the Ru solution in a multiwell plate. (b) Histogram of the individual pixel lifetimes in (a). (c) Time decay of image in (a) with all pixels binned, IRF, and monoexponential fit to the data with lifetime of 456 ns. (d-f) Living HeLa-cell labelled with ruthenium compound $Ru(dpp)_3^{2+}$ imaged with phosphor decay TCSPC at 54 kHz. (d) Phosphorescence intensity image obtained by single photon counting, (e) lifetime image with a lifetime distribution histogram (inset). (f) Decay data of all pixels binned. Biexponential fit yields a mean lifetime of 2.95 μs for $Ru(dpp)_3^{2+}$ and a 0.04 μs fast component for autofluorescence.

limit the length of the measurement window. Additionally, the invariant afterglow of the P20 phosphor decay means that at faster frame rates the photon event pixels are occupied longer, thus reducing the potential count rate and also the intensity of the photon events in each frame. To improve the time resolution further, a faster decay phosphor should be used.

The wide-field TCSPC imaging approaches described here are especially well suited for time-resolved imaging of transition metal complexes with typical lifetimes in the microsecond region,[8] including time-resolved luminescence anisotropy imaging.[10] They combine fast image acquisition within a few seconds with a low excitation power – well below 1 μW, i.e. more than 1000 times lower than reported previously with a sequential time-gating approach.[31,32] These techniques enable the collection of hundreds of photons per excitation cycle – even several photons after one excitation cycle per pixel, as long as they arrive in different frames.[14] In contrast to sequential gating techniques, no photons are lost. Due to the digital nature of photon counting and its associated advantages – e.g. Poisson statistics, a large dynamic range, a high time resolution, easy visualization of decays and the ability to perform meaningful multi- exponential decay analysis – they also have a better signal-to-noise ratio than frequency modulation techniques at low signal levels.[13] Picosecond resolution wide-field TCSPC can be performed with crossed-delay-line–, wedge-and-strip– or quadrant anodes,[33] which can typically detect one fluorescence photon per excitation pulse in the whole field of view, and a gain sweep method in an EBCCD has been proposed.[34,35] SPAD array detectors can also perform picosecond timing,[33,36,37] but for microsecond lifetimes the parallel detection of many photons per excitation pulse as performed here is beneficial. Another important consideration, especially with microsecond lifetimes and longer detection windows, is the dark noise performance of SPAD arrays, which is many orders of magnitude higher than MCP-based intensifiers, for which 0.02 events/sec/cm^2 have been quoted.[38]

5. CONCLUSION

Two wide-field TCSPC methods were successfully applied to imaging several transition metal complexes containing iridium and ruthenium with lifetimes around one microsecond. With conventional microsecond wide-field TCSPC there is a trade-off between a high frame rate and the number of pixels that can be imaged, and the time resolution is limited by the frame rate of the camera. We have demonstrated that the long-lived, invariant decay of the phosphor screen of the image intensifier can be exploited to find the photon arrival time within the frame exposure time. This not only improves the time resolution, but also allows bigger image size. This is relevant for general time-of-flight measurements, e.g. in lidar,[39,40] ion velocity mapping[20–22] or photon correlation techniques.[41]

The advantages of sensitive wide-field TCSPC imaging as presented here can be applied to imaging modalities such as simultaneous tracking and time decay measurements, TIRF, SAF or light-sheet microscopy, which are

difficult to implement with scanning techniques. By using a phosphor with a faster decay time to match a higher camera frame rate, the measurement of nanosecond decays could be possible with this technique.

ACKNOWLEDGMENTS

We would like to thank the UK's EPSRC Engineering Instrument Loan Pool, particularly Adrian Walker, for the loan of the Photron camera.

REFERENCES

1. P. Seitz and A. J. P. Theuwissen, *Single Photon Imaging*, Springer, Heidelberg, 2011.
2. K. K.-W. Lo, A. W.-T. Choi, and W. H.-T. Law, "Applications of luminescent inorganic and organometallic transition metal complexes as biomolecular and cellular probes," *Dalton T* **41**, pp. 6021–6047, 2012.
3. E. Baggaley, J. A. Weinstein, and J. A. G. Williams, "Lighting the way to see inside the live cell with luminescent transition metal complexes," *Coordin Chem Rev* **256**(15-16), pp. 1762–1785, 2012.
4. J.-C. G. Bünzli, "Lanthanide luminescence for biomedical analyses and imaging," *Chem Rev* **110**(5), pp. 2729–2755, 2010.
5. M. H. V. Werts, "Making sense of lanthanide luminescence," *Sci Prog* **88**(2), pp. 101–131, 2005.
6. N. A. Hosny, D. A. Lee, and M. M. Knight, "Single photon counting fluorescence lifetime detection of pericellular oxygen concentrations," *J Biomed Opt* **17**(1), p. 016007, 2012.
7. X.-D. Wang and O. S. Wolfbeis, "Optical methods for sensing and imaging oxygen: materials, spectroscopies and applications," *Chem Soc Rev* **43**, pp. 3666–3761, 2014.
8. R. I. Dmitriev and D. B. Papkovsky, "Optical probes and techniques for O_2 measurement in live cells and tissue," *Cell Mol Life Sci* **69**(12), pp. 2025–2039, 2012.
9. J. Kavandi, J. Callis, M. Gouterman, G. Khalil, D. Wright, E. Green, D. Burns, and B. McLachlan, "Luminescent barometry in wind tunnels," *Rev Sci Instrum* **61**(11), pp. 3340–3347, 1990.
10. E. Terpetschnig, H. Szmacinski, H. Malak, and J. R. Lakowicz, "Metal-ligand complexes as a new class of long-lived fluorophores for protein hydrodynamics," *Biophys J* **68**(1), p. 342350, 1995.
11. Z. Cao, C.-C. Huang, and W. Tan, "Nuclease resistance of telomere-like oligonucleotides monitored in live cells by fluorescence anisotropy imaging," *Anal Chem* **78**(5), pp. 1478–1484, 2006.
12. B. Valeur, *Fluorescence Spectroscopy in Biology*, vol. 3 of *Springer Series on Fluorescence*, ch. 2: Pulse and Phase Fluorometries: An Objective Comparison, pp. 30–48. Springer Berlin Heidelberg, 2005.
13. E. Gratton, S. Breusegem, J. Sutin, Q. Ruan, and N. Barry, "Fluorescence lifetime imaging for the two-photon microscope: time-domain and frequency-domain methods," *J Biomed Opt* **8**(3), pp. 381–390, 2003.
14. N. Sergent, J. A. Levitt, M. Green, and K. Suhling, "Rapid wide-field photon counting imaging with microsecond time resolution," *Opt Express* **18**(24), pp. 25292–25298, 2010.
15. L. M. Hirvonen, F. Festy, and K. Suhling, "Wide-field time-correlated single-photon counting (TCSPC) lifetime microscopy with microsecond time resolution," *Opt Lett* **39**(19), pp. 5602–5605, 2014.
16. P. Prosposito, D. Marks, H. Zhang, and M. Glasbeek, "Femtosecond double proton-transfer dynamics in [2,2-bipyridyl]-3,3-diol in solgel glasses," *J Phys Chem A* **102**(45), pp. 8894–8902, 1998.
17. J. G. Mainprize and M. J. Yaffe, "The effect of phosphor persistence on image quality in digital x-ray scanning systems," *Med Phys* **25**(12), pp. 2440–2454, 1998.
18. Z. Petrášek and K. Suhling, "Photon arrival timing with sub-camera exposure time resolution in wide-field time-resolved photon counting imaging," *Opt Express* **18**(24), pp. 24888–24901, 2010.
19. L. M. Hirvonen, Z. Petrášek, and K. Suhling, "Wide-field time-correlated single photon counting (TCSPC) microscopy with time resolution below the frame exposure time," *Nucl Instrum Meth A*, 2014. doi:10.1016/j.nima.2014.09.082
20. D. Strasser, X. Urbain, H. B. Pedersen, N. Altstein, O. Heber, R. Wester, K. G. Bhushan, and D. Zajfman, "An innovative approach to multiparticle three-dimensional imaging," *Rev Sci Instrum* **71**, pp. 3092–3098, 2000.

21. L. Dinu, A. T. J. B. Eppink, F. Rosca-Pruna, H. L. Offerhaus, W. J. van der Zande, and M. J. J. Vrakking, "Application of a time-resolved event counting technique in velocity map imaging," *Rev Sci Instrum* **73**, pp. 4206–4213, 2002.
22. C. Vallance, M. Brouard, A. Lauer, C. S. Slater, E. Halford, B. Winter, S. J. King, J. W. L. Lee, D. E. Pooley, I. Sedgwick, R. Turchetta, A. Nomerotski, J. J. John, and L. Hill, "Fast sensors for time-of-flight imaging applications," *Phys Chem Chem Phys* **16**, pp. 383–395, 2014.
23. K. Suhling, G. Hungerford, R. W. Airey, and B. L. Morgan, "A position-sensitive photon event counting detector applied to fluorescence imaging of dyes in sol-gel matrices," *Meas Sci Technol* **12**, pp. 131–141, 2001.
24. K. Suhling, R. W. Airey, and B. L. Morgan, "Optimisation of centroiding algorithms for photon event counting imaging," *Nucl Instrum Meth A* **437**(2-3), pp. 393–418, 1999.
25. L. M. Hirvonen, Z. Petrášek, A. Beeby, and K. Suhling, "Sub-μs time resolution wide-field time-correlated single photon counting (TCSPC) microscopy from photon event phosphor decay," *New J Phys* **accepted**, 2015.
26. P. R. Barber, S. M. Ameer-Beg, J. Gilbey, L. M. Carlin, M. Keppler, T. C. Ng, and B. Vojnovic, "Multiphoton time-domain fluorescence lifetime imaging microscopy: practical application to protein-protein interactions using global analysis," *J R Soc Interface* **6**(Suppl 1), pp. S93–S105, 2009.
27. https://www.assembla.com/spaces/ATD_TRI/wiki.
28. G. Zhou, C.-L. Ho, W.-Y. Wong, Q. Wang, D. Ma, L. Wang, Z. Lin, T. B. Marder, and A. Beeby, "Manipulating charge-transfer character with electron-withdrawing main-group moieties for the color tuning of iridium electrophosphors," *Adv Funct Mater* **18**(3), pp. 499–511, 2008.
29. A. Beeby, S. Bettington, I. D. W. Samuel, and Z. Wang, "Tuning the emission of cyclometalated iridium complexes by simple ligand modification," *J Mater Chem* **13**, pp. 80–83, 2003.
30. F. N. Castellano, J. D. Dattelbaum, and J. R. Lakowicz, "Long-lifetime Ru(II) complexes as labeling reagents for sulfhydryl groups," *Anal Biochem* **255**(2), pp. 165–170, 1998.
31. N. Gahlaut and L. W. Miller, "Time-resolved microscopy for imaging lanthanide luminescence in living cells," *Cytom Part A* **77A**(12), pp. 1113–1125, 2010.
32. K. Hanaoka, K. Kikuchi, S. Kobayashi, and T. Nagano, "Time-resolved long-lived luminescence imaging method employing luminescent lanthanide probes with a new microscopy system," *J Am Chem Soc* **129**(44), pp. 13502–13509, 2007.
33. X. Michalet, R. Colyer, G. Scalia, A. Ingargiola, R. Lin, J. E. Millaud, S. Weiss, O. H. Siegmund, A. S. Tremsin, J. V. Vallerga, A. Cheng, M. Levi, D. Aharoni, K. Arisaka, F. Villa, F. Guerrieri, F. Panzeri, I. Rech, A. Gulinatti, F. Zappa, M. Ghioni, and S. Cova, "Development of new photon-counting detectors for single-molecule fluorescence microscopy," *Philos T R Soc B* **368**, p. 1611, 2013.
34. L. M. Hirvonen, S. Jiggins, N. Sergent, G. Zanda, and K. Suhling, "Photon counting imaging with an electron-bombarded CCD: towards a parallel-processing photoelectronic time-to-amplitude converter," *Rev Sci Instrum* **85**(12), p. 123102, 2014.
35. L. M. Hirvonen, S. Jiggins, N. Sergent, G. Zanda, and K. Suhling, "Photon counting imaging with an electron-bombarded CCD: towards wide-field time-correlated single photon counting (TCSPC)," *Nucl Instrum Meth A* **accepted**, 2015.
36. S. P. Poland, N. Krstajić, S. Coelho, D. Tyndall, R. J. Walker, V. Devauges, P. E. Morton, N. S. Nicholas, J. Richardson, D. D.-U. Li, K. Suhling, C. M. Wells, M. Parsons, R. K. Henderson, and S. M. Ameer-Beg, "Time-resolved multifocal multiphoton microscope for high speed FRET imaging *in vivo*," *Opt Lett* **39**(20), pp. 6013–6016, 2014.
37. S. P. Poland, N. Krstajić, J. Monypenny, S. Coelho, D. Tyndall, R. J. Walker, V. Devauges, J. Richardson, N. Dutton, P. Barber, D. D.-U. Li, K. Suhling, T. Ng, R. K. Henderson, and S. M. Ameer-Beg, "A high speed multifocal multiphoton fluorescence lifetime imaging microscope for live-cell FRET imaging," *Biomed Opt Express* **6**(2), pp. 277–296, 2015.
38. O. H. Siegmund, "High-performance microchannel plate detectors for UV/visible astronomy," *Nucl Instrum Meth A* **525**(1-2), pp. 12–16, 2004.

39. G. S. Buller and A. M. Wallace, "Ranging and three-dimensional imaging using time-correlated single-photon counting and point-by-point acquisition," *IEEE J Sel Top Quant* **13**(4), pp. 1006–1015, 2007.
40. A. McCarthy, R. J. Collins, N. J. Krichel, V. Fernandez, A. M. Wallace, and G. S. Buller, "Long-range time-of-flight scanning sensor based on high-speed time-correlated single-photon counting," *Appl Optics* **48**(32), pp. 6241–6251, 2009.
41. L. Turgeman and D. Fixler, "Time-averaged fluorescence intensity analysis in fluorescence fluctuation polarization sensitive experiments," *Biomed Opt Express* **4**(6), pp. 868–884, 2013.